

Experimental and Simulation Study on Heat Accumulation Phenomenon at the Bottom of Solid Thermal Storage Electric Boilers



Yichao Wang^{1,2}, Sai Liu^{1,2}, Yiwei Yang^{1,2}, Fenfei Qiao³, Yong Sun^{1,2*}

¹ Hebei Energy Storage Heating Technology Innovation Center, Zhangjiakou 075024, China

² Department of Energy Engineering, Hebei University of Architecture, Zhangjiakou 075024, China

³ Hebei Jianto Xuanhua Thermal Power Co. Ltd., Zhangjiakou 075100, China

Corresponding Author Email: sunyong@hebiace.edu.cn

Copyright: ©2024 The authors. This article is published by IETA and is licensed under the CC BY 4.0 license (<http://creativecommons.org/licenses/by/4.0/>).

<https://doi.org/10.18280/ijht.420631>

ABSTRACT

Received: 9 May 2024

Revised: 28 September 2024

Accepted: 17 October 2024

Available online: 31 December 2024

Keywords:

solid thermal storage electric boiler, heat accumulation phenomenon, experiment, numerical simulation

This paper addresses the issue of heat accumulation and low heat release efficiency at the bottom of solid thermal storage electric boilers through experimental and simulation studies. A test platform was designed for conducting three sets of comparative experiments. A numerical simulation model was established and solved, and the scientific accuracy of the research was verified through a comparison of experimental data and simulation results. The study shows that as the thermal storage and release processes progress, the temperature of the thermal insulation structure at the bottom of the storage body gradually increases, with significant heat accumulation. Under the experimental scale, the accumulated heat reaches $5.25e^5$ kJ. Improving ventilation conditions does not enhance the heat utilization of this part. Calculations indicate that the thermal energy in the insulation brick layer is approximately ten times greater than that of other brick layers, playing a dominant role. With three cycles of thermal storage and release, the accumulated heat is substantial, offering considerable potential for improvement.

1. INTRODUCTION

The "carbon peak and carbon neutrality" policy was firstly put forward in the Chinese Central Economic Work Conference 2020 which aiming at reducing the carbon emission in China. According to this policy, the carbon emissions should reach their peak before 2030 and achieve neutrality before 2060. For this purpose, the adjustment and optimization of industrial and energy structures should be accelerated to promote the efficient heating systems. Against this backdrop, using clean electricity as a heat source, adding energy storage between the electricity and heating systems, can reduce the conflict between grid peak shaving and heating supply to a certain extent while ensuring electricity supply for heating. Solid electric thermal storage technology can convert fluctuating electricity from low grid valleys, wind power, and other sources into thermal energy, which is used for heating during peak electricity demand periods. This is an advanced and efficient form of thermal storage, playing a crucial role in improving the flexibility of the power grid.

Domestic and international experts have conducted extensive research on solid thermal storage electric boilers through numerical simulations and experimental tests, focusing on thermal storage and release characteristics, economics, operation modes, evaluation indices, and system optimization. These efforts have driven the technological advancement of solid thermal storage electric boilers [1-5]. However, as a new heating method, solid thermal storage technology faces many engineering challenges in practical

applications, and research in related fields is limited. This project aims to address the practical operational issues of solid thermal storage electric boilers, taking a novel approach with innovative aspects.

At the initial stage of heat release in solid thermal storage electric boilers, the temperature of the thermal storage bricks reaches 500-700°C, and the heat exchange between the air and the thermal storage bricks is efficient, resulting in good heating performance. As the heat release process continues, the average brick temperature of the thermal storage body decreases, significantly reducing energy quality and resulting in poor heating performance. In engineering practice, methods such as increasing the boiler's thermal storage temperature are commonly used to enhance the heat release capacity of the thermal storage body. However, this approach consumes large amounts of energy, presents challenges to the safe and stable operation of the electric heating system, and is economically inefficient. Therefore, it is particularly important to improve the thermal efficiency of solid thermal storage electric boilers based on the existing operating parameters.

This study mainly analyzes the heat accumulation phenomenon at the bottom of solid thermal storage electric boilers using experimental and simulation methods. Chapter 1 introduces the application background and main technical issues of solid thermal storage electric boilers. Chapter 2 presents the experimental study on the heat accumulation phenomenon at the bottom of solid thermal storage electric boilers. Chapter 3 introduces the numerical simulation study on the heat accumulation phenomenon at the bottom of solid

thermal storage electric boilers. Chapter 4 compares the experimental data with simulation results and evaluates the experimental platform and numerical calculation model. Chapter 5 presents the research conclusions and suggestions for future studies.

2. EXPERIMENT

2.1 Working principle of solid thermal storage electric boiler

The solid thermal storage electric boiler consists of a heating device, thermal storage device, air circulation system, water circulation system, control system, and other supporting devices. Figure 1 is the workflow diagram of the solid thermal storage electric boiler. The thermal storage process involves the electric heating wire being powered, generating heat through the electric heating effect, and storing it in the MgO-rich thermal storage bricks. During the heating process, the air valve and fan are opened in sequence, and the circulating air carries the heat from the thermal storage bricks. This heat is transferred to the heating system's circulating water system through the heat exchanger, completing the heating task [6].

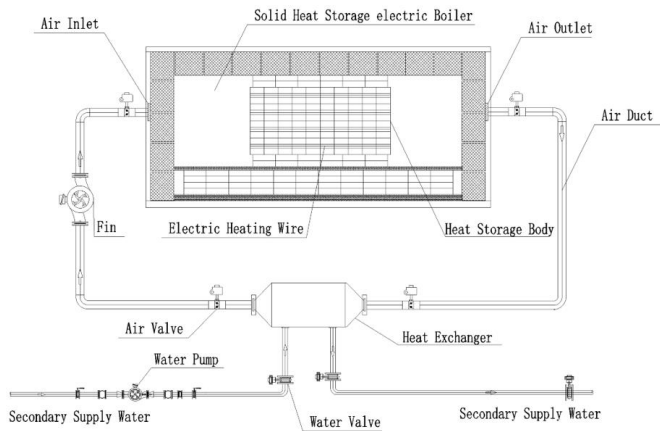


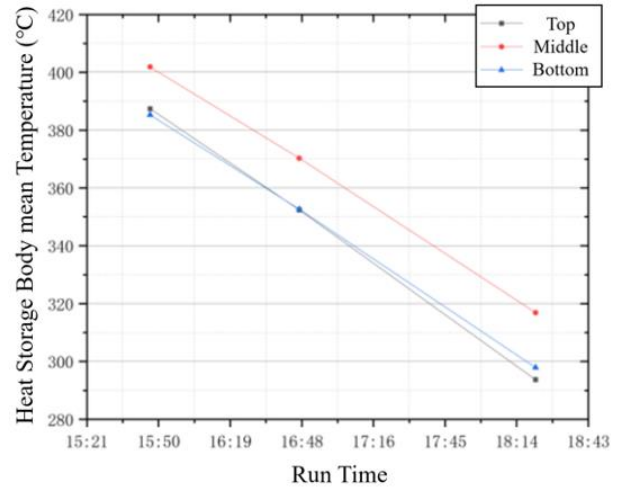
Figure 1. Workflow diagram of solid thermal storage electric boiler

2.2 Discovery of heat accumulation phenomenon

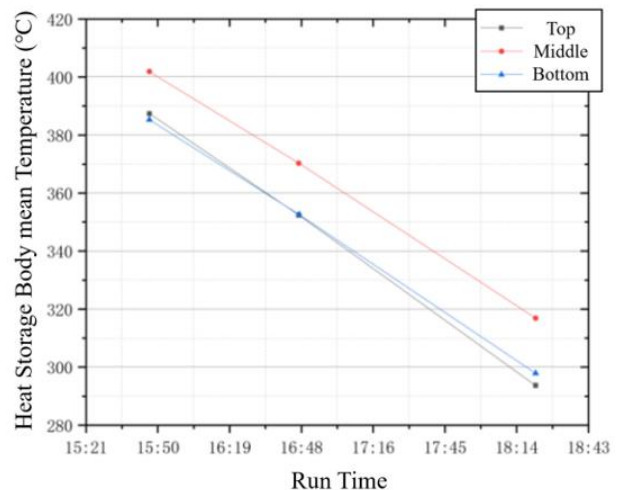
The solid thermal storage electric boiler system is widely used in northern China. This study investigates a real engineering case located in Wanquan District, Zhangjiakou City, China. Due to spatial and system operation safety requirements, three measurement points were set vertically within the thermal storage body: upper, middle, and lower levels. The temperature variation at these measurement points was tested during the first and last three hours of one thermal release cycle, as shown in Figure 2.

Through analysis of the figure, it can be observed that during the early stage of heat release, the highest temperature in the thermal storage body is at the middle, while the upper and lower parts have slightly lower temperatures due to heat dissipation to the surrounding environment. Looking at the overall heat release process, in the first three hours of heat release, the average temperature drop at the upper, middle, and lower measurement points ranges from 85°C to 95°C. Since the heat released is much greater than the internal heat conduction, the heat release within the entire thermal storage

body is uniform. In the final three hours of heat release, the average temperature of the three measurement points drops significantly, with temperature changes ranging from 1°C to 7°C, and the heat release capability decreases significantly. The temperature distribution changes from high to low as the upper, middle, and lower points. Within three hours, the temperature at the upper measurement point remains almost unchanged and shows a downward trend, while the temperatures at the middle and lower points gradually increase. Internal heat conduction within the thermal storage body takes a dominant role, and heat accumulates from the upper part to the middle and lower parts.



(a) Early stage of heat release



(b) End stage of heat release

Figure 2. Average temperature of thermal storage body at different depths before and after heat release in solid thermal storage electric boiler

2.3 Experimental analysis of bottom heat accumulation phenomenon

To further analyze the bottom heat accumulation issue in the solid thermal storage electric boiler system, a test platform was built.

2.3.1 Test platform introduction

The experimental testing platform is designed with a thermal power of 85 kW, and the heating mode is a fan coil. The thermal storage body is mainly composed of eight layers

of MgO-based thermal storage bricks, each containing 92% MgO. To enhance heat transfer, the thermal storage bricks are arranged in rows with gaps facing the wind. Each thermal storage brick has three semi-circular grooves with a diameter of 0.055 m on one side. Two thermal storage bricks are combined to form three circular channels, which are used to place spiral resistive heating wires. The bottom of the thermal storage body is equipped with support and insulation structures. From top to bottom, there are four layers of unperforated magnesium oxide bricks, a single layer of clay

bricks (referred to as clay bricks (1)), and a double layer of clay bricks (referred to as clay bricks (2)). Each layer is separated by aluminosilicate fiber insulation mats. The top and sides of the thermal storage body are insulated with 0.25 m thick aluminosilicate fiber insulation cotton, and the entire thermal storage body is enclosed in a steel shell. The heat exchanger, fan, and water pump are arranged above the thermal storage body, with three air inlet channels and one air outlet channel. The air vents are located on both sides of the thermal storage body, as shown in Figure 3.



a) Boiler Appearance



b) Inside of the Boiler

Figure 3. Experimental device

Other main equipment parameters are listed in the Table 1 below:

Table 1. Main equipment list

Equipment Name	Quantity	Remarks
Solid Thermal Storage Electric Boiler	1	Electric heating wire power 85 kW; thermal storage capacity 514 kW·h
Circulating Fan	1	20 spiral iron-chromium-aluminum heating wires; 400 thermal storage bricks (5×8×10)
Circulating Water Pump	1	Airflow 5268 m ³ /h; total pressure 1758 Pa; power 3 kW
Heat Pipe Heat Exchanger	1	Flow rate 4 m ³ /h; head 15 m; power 0.37 kW
Fan Coil Heater	6	Heat exchange area 23.5 m ² ; dimensions: 0.6×0.6×0.56 m; 72 high-frequency welded carbon steel fins

2.3.2 Experimental setup

To monitor the temperature inside the thermal storage body, measurement points were set at three layers along the direction of airflow: front (T_{1x}), middle (T_{2x}), and rear (T_{3x}). Each layer was evenly distributed with nine measurement points (T_{x1}-T_{x9}), as shown in Figure 4.

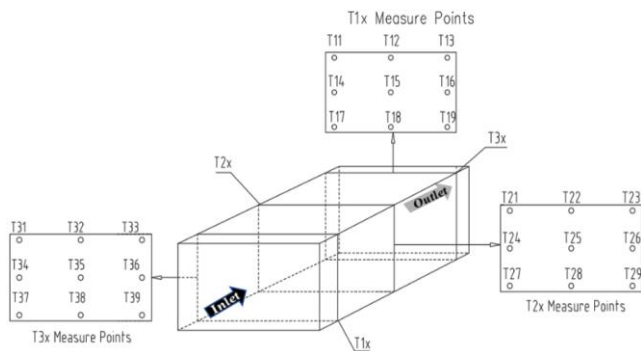


Figure 4. Distribution of measurement points

Other testing instruments are listed in Table 2 below:

Table 2. Main testing sensors

Instrument Type	Model	Range	Description
Temperature Sensor	K-type Thermocouple	0-1000°C	Length: 0.5m, 0.7m, 1m
Pressure Sensor	Analog	0-0.1MPa	
Thermometer		0-1000°C	
Flowmeter		0-15m ³ /h	Accuracy 0.5 level, pressure range 4.0 MPa
Pressure Gauge	YE-75	0-10kPa	

To test the basic operational characteristics of the system and provide fundamental data for subsequent numerical simulations and system modifications, three rounds of continuous heat storage and release experiments were designed. Temperature and flow velocity data at each measurement point were recorded. Specifically:

(1) The thermal storage system begins operation from room temperature, with weak ventilation during the first round of heat storage. Heating is stopped when the central temperature of the thermal storage body reaches 500°C. The middle air inlet is then opened, and the fan power is increased for heat release. The heat release duration is 10 hours, constituting the first round of heat release.

(2) After the first round of heat release ends, the electric heating is restarted, the fan frequency is reduced, and basic ventilation is maintained for the second round of heat storage. The process is similar to (1), with heating stopped when the thermal storage body center reaches 500°C, and then the second round of heat release occurs.

(3) After the second round of heat release ends, the same procedure as (2) is followed for the third round of heat storage. All three air inlet channels are opened, and the fan power is increased for heat release, with a heat release duration of 10 hours for the third round of heat release.

3. SIMULATION

3.1 Physical model

In order to visually observe and analyze the heat accumulation phenomenon at the bottom of the thermal storage body, this study builds a model based on the experimental setup of the solid thermal storage electric boiler, as shown in Figure 5.

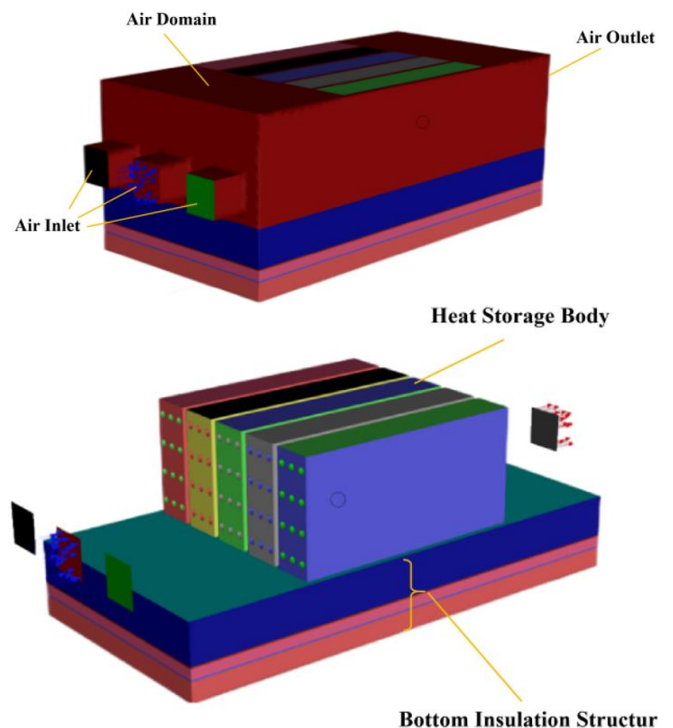


Figure 5. 3D view of solid thermal storage electric boiler model

3.2 Mathematical model

The fluid flow and heat transfer processes involved in this study follow the basic physical laws of mass conservation, momentum conservation, and energy conservation. The k-ε turbulence model is used for solving [7, 8].

(1) Mass conservation—Continuity equation

$$\frac{\partial \rho}{\partial t} + \frac{\partial(\rho u)}{\partial x} + \frac{\partial(\rho v)}{\partial y} + \frac{\partial(\rho w)}{\partial z} = 0 \quad (1)$$

For incompressible fluids with constant density, the continuity equation simplifies to:

$$\frac{\partial(u)}{\partial x} + \frac{\partial(v)}{\partial y} + \frac{\partial(w)}{\partial z} = 0 \quad (2)$$

(2) Momentum conservation law—N-S equations

$$\begin{aligned} u \frac{\partial(\rho u)}{\partial x} + v \frac{\partial(\rho u)}{\partial y} + w \frac{\partial(\rho u)}{\partial z} \\ = -\frac{\partial p}{\partial x} + \frac{\partial}{\partial x} \left(\mu \frac{\partial u}{\partial x} \right) + \frac{\partial}{\partial y} \left(\mu \frac{\partial u}{\partial y} \right) \\ + \frac{\partial}{\partial z} \left(\mu \frac{\partial u}{\partial z} \right) \end{aligned} \quad (3)$$

$$\begin{aligned} u \frac{\partial(\rho v)}{\partial x} + v \frac{\partial(\rho v)}{\partial y} + w \frac{\partial(\rho v)}{\partial z} \\ = -\frac{\partial p}{\partial y} + \frac{\partial}{\partial x} \left(\mu \frac{\partial v}{\partial x} \right) + \frac{\partial}{\partial y} \left(\mu \frac{\partial v}{\partial y} \right) \\ + \frac{\partial}{\partial z} \left(\mu \frac{\partial v}{\partial z} \right) \end{aligned} \quad (4)$$

$$\begin{aligned} u \frac{\partial(\rho w)}{\partial x} + v \frac{\partial(\rho w)}{\partial y} + w \frac{\partial(\rho w)}{\partial z} \\ = -\frac{\partial p}{\partial z} + \frac{\partial}{\partial x} \left(\mu \frac{\partial w}{\partial x} \right) + \frac{\partial}{\partial y} \left(\mu \frac{\partial w}{\partial y} \right) \\ + \frac{\partial}{\partial z} \left(\mu \frac{\partial w}{\partial z} \right) - \rho g \end{aligned} \quad (5)$$

(3) Energy conservation equation—Heat transfer differential equation

$$\frac{\partial T}{\partial t} + \nabla \cdot (uT) = \alpha \nabla^2 T + Q' \quad (6)$$

For conditions without internal heat sources and constant properties, this simplifies to:

$$\begin{aligned} \frac{\partial(\rho T)}{\partial t} + \frac{\partial(\rho u T)}{\partial x} + \frac{\partial(\rho v T)}{\partial y} + \frac{\partial(\rho w T)}{\partial z} \\ = \frac{\partial}{\partial x} \left(\frac{\lambda}{C_p} \frac{\partial T}{\partial x} \right) + \frac{\partial}{\partial y} \left(\frac{\lambda}{C_p} \frac{\partial T}{\partial y} \right) \\ + \frac{\partial}{\partial z} \left(\frac{\lambda}{C_p} \frac{\partial T}{\partial z} \right) \end{aligned} \quad (7)$$

(4) k-ε equations:

$$\frac{\partial(\rho k)}{\partial t} + \frac{\partial(\rho k u_i)}{\partial x_i} = \frac{\partial}{\partial x_j} \left[\left(\mu + \frac{\mu_t}{\sigma_k} \right) \frac{\partial k}{\partial x_j} \right] + G_k + G_b - \rho \epsilon - Y_M + S_k \quad (8)$$

$$\begin{aligned} \frac{\partial(\rho \epsilon)}{\partial t} + \frac{\partial(\rho \epsilon u_i)}{\partial x_i} = \frac{\partial}{\partial x_j} \left[\left(\mu + \frac{\mu_t}{\sigma_\epsilon} \right) \frac{\partial \epsilon}{\partial x_j} \right] \\ + C_{1\epsilon} \frac{\epsilon}{k} (G_k + C_{3\epsilon} G_b) - C_{2\epsilon} \rho \frac{\epsilon^2}{k} + S_\epsilon \end{aligned} \quad (9)$$

3.3 Simulation calculation

This study uses ANSYS software for the 3D modeling and calculation of the solid thermal storage electric boiler, with the

Fluent solver calculating temperature and velocity distribution of the model. For simplification, reasonable assumptions for the solid thermal storage electric boiler model are made as follows [9-12]:

- (1) Air is incompressible and viscous, and the flow in the air duct is turbulent;
- (2) Radiation heat transfer is not considered in the model;
- (3) The inlet air temperature and flow velocity are constant during each heat storage and release stage;
- (4) Relevant system physical parameters are constant;
- (5) The temperature and pressure inside the thermal storage body change over time;
- (6) Heat transfer from the thermal storage body to the surroundings is ignored.

When dividing the physical model into meshes, the mesh for the thermal storage body insulation structure at the bottom is refined. After a mesh independence verification, the total mesh number is 3,549,724, with a minimum orthogonality quality of 0.2, as shown in Figure 6.

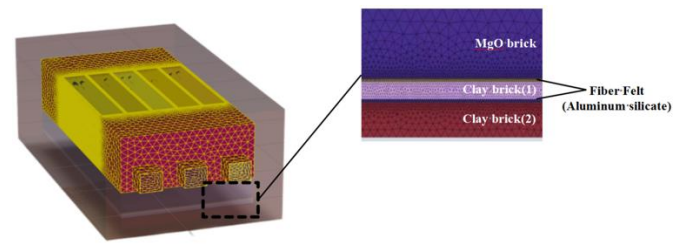


Figure 6. Physical model mesh division

The material property parameters for the main materials involved in the calculation are as follows [13-15] (Table 3).

Table 3. Main material property parameters

Name	Specific Heat Cp (J/kg·K)	Density (kg/m ³)	Thermal Conductivity λ (W/m·K)	Remarks
Magnesium Oxide Brick	1000	2796	7.27	Thermal storage body
Air	1006.43	1.225	0.0242	
Alumina Fiber	900	128	0.084	Insulation felt
Clay Brick	960	1800	1.07	

Based on the experimental conditions in Section 3.2, the simulation process is set with the following inlet wind speed, wind temperature, and heat storage/release duration (Table 4).

3.4 Simulation results analysis

This section analyzes the temperature change of the thermal storage body and the heat accumulation issue during the three rounds of heat storage and release.

After the first round of heat storage and release, the temperature distribution of the solid thermal storage electric boiler in the central cross-section parallel to the airflow direction is shown in Figure 7.

As shown in Figure 7(a), during the first round of heat storage, the thermal storage body increases from the initial temperature (14°C) after 6.5 hours of heating with a small amount of ventilation. The highest temperature reaches 503°C, and the average temperature of the thermal storage body rises

from 14°C to 366.9°C. The heat storage center is located at the top, rear part of the thermal storage body (along the direction of airflow). The insulation structure at the bottom of the thermal storage body shows a noticeable temperature rise. As shown in Figure 7(b), after 10 hours of heat release, the average temperature of the thermal storage bricks decreases to

115.4°C. The internal temperature distribution becomes relatively uniform, and the average temperature of the insulation structure at the bottom is higher than that of the thermal storage body, indicating that heat continues to be stored in the insulation structure and should not dissipate.

Table 4. Inlet wind speed and wind temperature settings for each stage

Heat Storage/Release Process	Inlet Wind Speed (m/s)	Inlet Wind Temperature (°C)	Duration (s)	Remarks
First Round Heat Storage	1.84	24.17	23400	Heat storage temperature is 500°C; during the first two rounds of heat release, only the middle wind inlet is opened.
First Round Heat Release	5.93	85.47	36000	
Second Round Heat Storage	1.38	32.98	19800	In the third round of heat release, all three wind inlets are opened; heat release duration is 10 hours.
Second Round Heat Release	5.86	91.74	36000	
Third Round Heat Storage	1.29	37.95	21600	
Third Round Heat Release	6.11	95.84	36000	

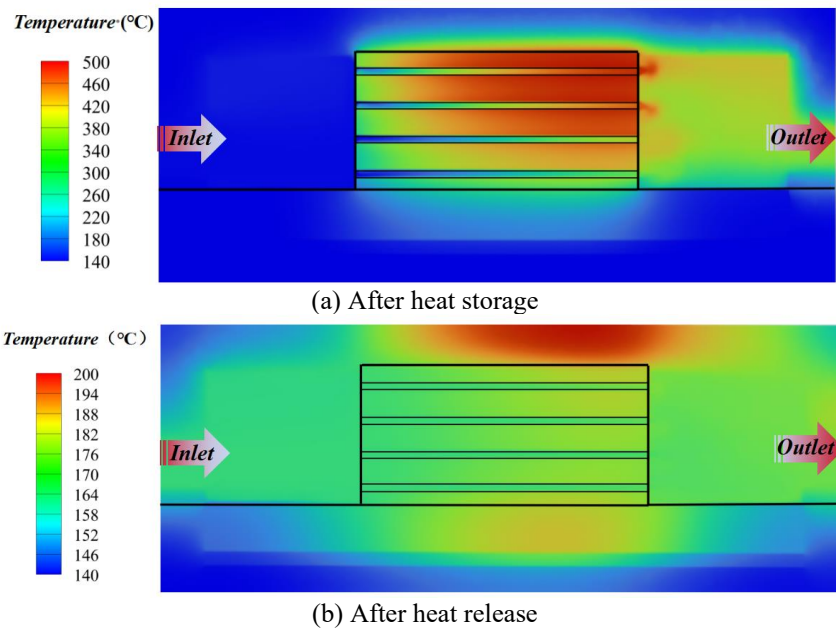


Figure 7. Temperature distribution of the boiler center section at the end of the first round of heat storage and heat release

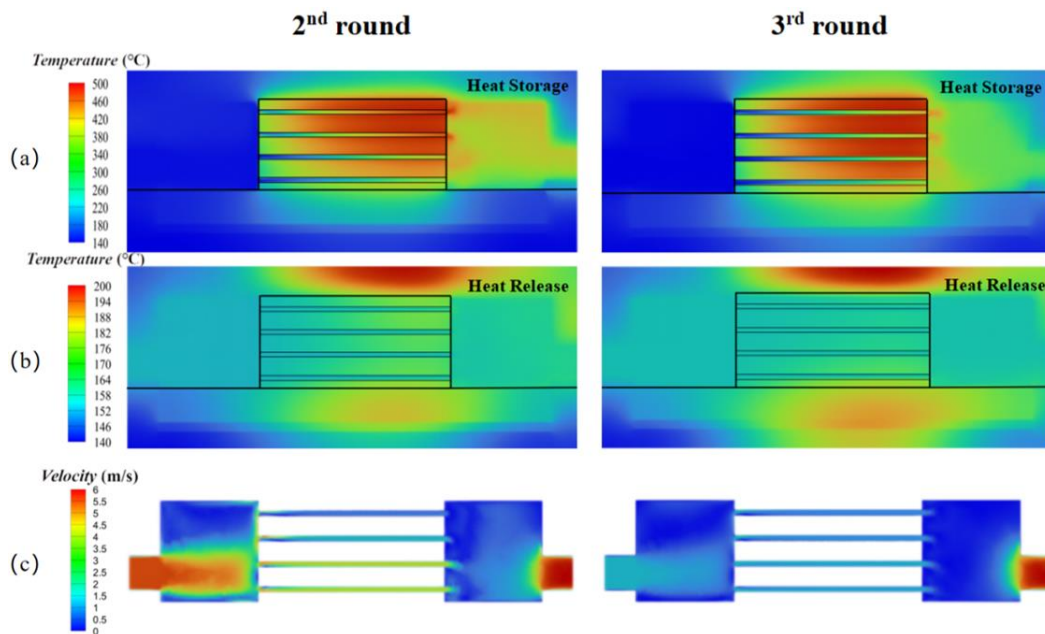


Figure 8. Temperature and ventilation speed distribution at the furnace center section after the second and third rounds of heat storage and release

Figure 8 shows the temperature and airflow velocity distribution in the central cross-section of the boiler at the end of the second and third rounds of heat storage and release. From this, we can see that, after the second round of heat storage, the highest temperature of the thermal storage body reaches 558°C, with an average temperature of 418.5°C, which is 51.6°C higher than the average temperature of the first round of heat storage. This indicates that the first round of heat storage and release, where only the middle wind inlet was opened, resulted in slower airflow in the upper channel of the thermal storage body (as shown in Figure 8(c)). As a result, heat could not be sufficiently carried away by the air, and heat accumulated in the upper rear area of the thermal storage body, leading to an increase in the average temperature. The temperature distribution of the thermal storage body became uneven, causing the heat exchange capacity and heat exchange efficiency of certain areas to decrease, reducing the overall heat storage and release capacity, lowering the air quality, and affecting the system's heat efficiency and economy. During the third round of heat storage and release, all three air inlets were opened, and as shown in Figure 8(c), the airflow distribution inside the air ducts became more uniform. After the third round of heat storage, the average temperature of the thermal storage bricks reached 367.7°C, and the overall temperature distribution of the thermal storage body became more uniform, alleviating the heat accumulation phenomenon. The system's operational efficiency and economy were improved.

By comparing the temperature distribution of the insulation structure at the bottom of the thermal storage body after the three rounds of heat storage and release, it can be concluded that, as the heat storage and release cycles proceed, heat is transferred from the thermal storage body to the bottom insulation structure, causing the temperature of the insulation structure to gradually increase. The wind speed and uniformity of the air supply during heat storage and release do not significantly affect the temperature rise effect. The heat accumulation phenomenon is persistent and difficult to eliminate.

In order to further analyze the characteristics of heat accumulation in the insulation structure at the bottom of the heat storage body, the temperature cloud maps of the cross-sections of the insulation structure below the heat storage body, i.e., the four layers of unperforated MgO bricks, clay bricks (1), and clay bricks (2), at the end of the three rounds of heat release are summarized, as shown in Figure 9.

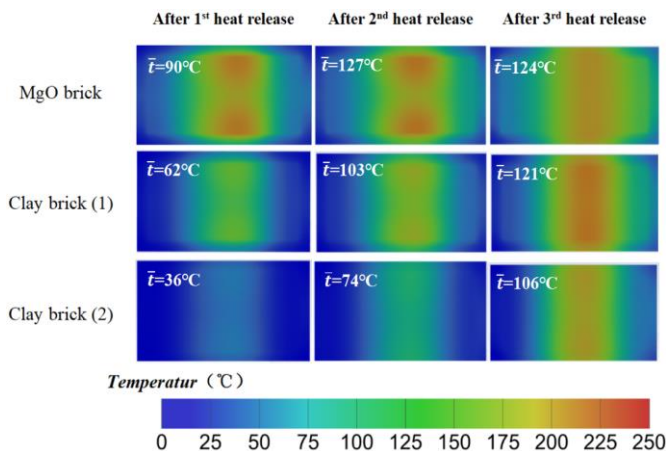


Figure 9. Temperature distribution at different positions at the bottom after the heat release of the solid heat storage electric boiler

After completing the three rounds of heat storage and release, the overall temperature of the insulation structure at the bottom of the heat storage body gradually increases. Heat is transmitted from top to bottom in the vertical direction, gradually accumulating. By comparing the MgO brick cloud maps after the second and third rounds of heat release, it can be seen that although improving the air supply uniformity can slightly reduce the average temperature of the bricks and reduce the temperature gradient of the MgO brick layer, it has little effect on alleviating the heat accumulation in the insulation structure. Analyzing the temperature cloud maps of the three insulation layers after the third heat release, it is predicted that if the heat storage and release process continues for multiple rounds, the entire insulation structure will be gradually heated, with temperatures tending to equalize, and the average temperature (\bar{t}) will exceed 100°C, with the highest temperature exceeding 200°C.

Based on the above simulation results, the conclusion can be drawn that after several rounds of heat storage and release, a large amount of heat accumulates in the insulation structure at the bottom of the heat storage body, and this heat is of higher quality, which cannot be easily utilized by changing the airflow organization or system operation mode. Adopting other improvement measures to utilize this heat is economically viable and has research value [16, 17].

3.5 Calculation of accumulated heat at the bottom of the heat storage body

Based on the simulation results, the maximum heat generated at the furnace bottom during the three rounds of heat storage and release is considered.

$$\Sigma Q_{\max} = \Sigma Q_1 + \Sigma Q_2 + \Sigma Q_3 \quad (10)$$

where:

ΣQ_1 — Total heat stored in the standard MgO brick layer during the three rounds of heat storage and release, kJ

ΣQ_2 — Total heat stored in the middle clay insulation brick layer during the three rounds of heat storage and release, kJ

ΣQ_3 — Total heat stored in the bottom clay insulation brick layer during the three rounds of heat storage and release, kJ

The temperature variation of the three brick layers during the three rounds of heat storage and release is obtained from the simulation results. By using the physical parameters of different brick layers and the brick layer volumes, the mass of each part of the bricks is calculated. Then, by utilizing the temperature changes of the brick layers every minute, the heat stored in the brick layers per minute is obtained. The total heat stored in the brick layers at different positions at the bottom of the heat storage body during the entire heat storage and release process is summed. Taking the heat release of the standard MgO brick layer per minute as an example:

$$Q_1 = C_{p1} M_1 \Delta t_1 \quad (11)$$

where:

Q_1 — Heat stored in the standard MgO brick layer per minute, kJ

C_{p1} — Specific heat capacity of the standard MgO brick, J/(kg·K)

M_1 — Total mass of the standard MgO brick layer, kg

Δt_1 — Average temperature change per minute of the standard MgO brick layer, K

The calculations for other brick layers are performed similarly. Finally, the results obtained are as follows:

$$\Sigma Q_1 = 7.26e^5 kJ, \Sigma Q_2 = 6.57e^4 kJ, \Sigma Q_3 = 9.63e^4 kJ$$

From the calculation results, it can be seen that the heat accumulation in the MgO brick layer is the largest, about 10 times that of the other two brick layers. Therefore, fully utilizing the heat stored in the MgO brick layer has a significant effect on improving the system's heat efficiency. During the three rounds of heat storage and release in the solid heat storage electric boiler, the total heat stored in the bottom standard brick layer and the clay insulation brick layer is about $5.25e^5$ kJ.

4. COMPARISON OF EXPERIMENTAL AND SIMULATION DATA

To evaluate the operational performance of the experimental device and the accuracy of the simulation model, the maximum and average temperature data of the heat storage body during the three rounds of heat storage and release were selected for comparison. The results are shown in Figures 10 and 11:

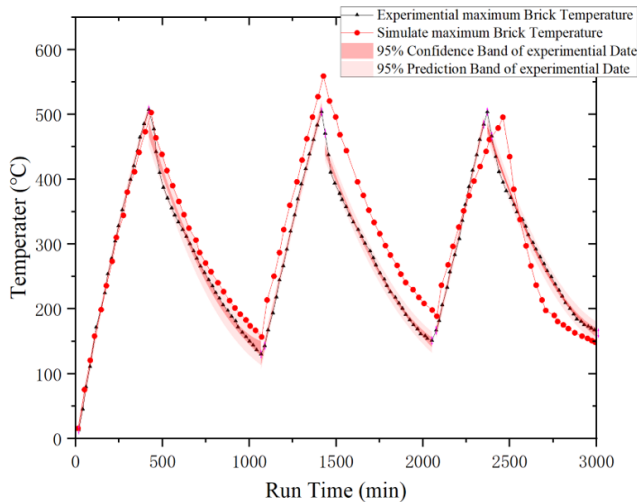


Figure 10. Maximum brick temperature in three rounds of heat storage and release (Experimental vs. Simulation)

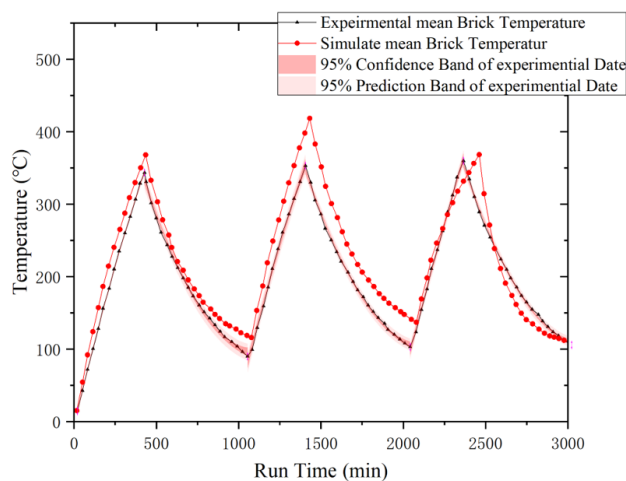


Figure 11. Average brick temperature in three rounds of heat storage and release (Experimental vs. Simulation)

During the experimental process, the heat storage cutoff temperature of the solid heat storage electric boiler was set to 500°C. The first round of heat storage was observed to take 5 hours and 20 minutes. In the simulation, the first round of heat storage was completed in 5 hours and 30 minutes, and the maximum temperature of the heat storage body reached 503°C. The experimental data and simulation results match well. As the heat storage and release process continues, the error between the experimental data and simulation results gradually increases. The average error of the maximum temperature and average temperature during the three rounds of heat storage and release is 6.08% and 9.33%, respectively [18-20].

In conclusion, the system operation characteristics of the experimental device can be well described by the simulation, and the design of the experimental device meets the research needs. The simulation model and results accurately reflect the real heat transfer and fluid flow processes, laying the foundation for future research on the heat recovery system at the bottom of the boiler.

5. CONCLUSIONS AND PROSPECTS

This research starts with the working principle of the solid heat storage electric boiler and, based on analyzing the physical process of heat storage and release, uses experimental and simulation methods to study the heat accumulation problem at the bottom of the heat storage body. First, a test platform was established for the heat accumulation phenomenon at the bottom of the solid heat storage boiler, and three rounds of experimental testing were conducted. Then, using the test platform as a prototype, a physical model and mathematical model for numerical simulation were established and calculated. Finally, by comparing and analyzing the experimental data and simulation results, the scientificity and accuracy of the experiments and simulations were verified. The main conclusions of this study are:

(1) Through the analysis of experimental and simulation data, the temperature of the heat storage body and the insulation structure at the bottom gradually rises as the heat storage and release process continues, and heat accumulation occurs. Improving the ventilation conditions can optimize the temperature distribution of the heat storage body and effectively reduce its temperature non-uniformity, but the effect of changing ventilation conditions on the heat utilization in the insulation structure is minimal.

(2) Calculations show that the heat accumulation phenomenon in the standard heat storage brick layer of the boiler's insulation structure is the most serious, one order of magnitude higher than in other brick layers. The total heat storage in the insulation structure is $5.25e^5$ kJ. Fully utilizing the heat stored in the standard heat storage brick is the most effective way to alleviate the heat accumulation phenomenon.

(3) By comparing the simulation results and experimental data, the experimental and simulation data match well. In the experiment, it took 5 hours and 20 minutes to heat the solid heat storage electric boiler from room temperature to 500°C. In the simulation, this heating process was calculated to take 5 hours and 30 minutes. The average error of the average temperature during the three rounds of heat storage and release was less than 10%.

The results of this study show that the heat accumulation effect at the bottom of the solid heat storage boiler cannot be

effectively alleviated by changing the airflow and operation modes. Future research is recommended to design a heat recovery system at the bottom, such as setting up a coil heat exchanger in the insulation structure at the bottom, which is connected to municipal water to carry away the accumulated heat, thus effectively improving the system's heat utilization. However, the layout of the coils and the application of recovered heat still require further research.

ACKNOWLEDGEMENTS

This paper was supported by Science and Technology Project of Hebei Education Department (Grant No.: QN2023076); Hebei Innovation Capability Improvement Project (Grant No.: 19244503D).

REFERENCES

- [1] Boshell, F., Salgado, A., Goussous, N., Ravishankar, M., Richards, O., Walker, J., Buchanan, F. (2020). Innovation outlook: Thermal energy storage.
- [2] Laing, D., Lehmann, D., Fiß, M., Bahl, C. (2009). Test results of concrete thermal energy storage for parabolic trough power plants. *Journal of Solar Energy Engineering*, 131(4): 041007. <https://doi.org/10.1115/1.3197844>
- [3] Hua, Y.C., Zhao, T., Guo, Z.Y. (2017). Transient thermal conduction optimization for solid sensible heat thermal energy storage modules by the Monte Carlo method. *Energy*, 133: 338-347. <https://doi.org/10.1016/j.energy.2017.05.073>
- [4] Osintsev, K., Aliukov, S., Kuskarbekova, S. (2021). Investigation of operation of coil-flow steam generator of serpentine type in conditions of low ambient temperatures. *International Journal of Heat and Technology*, 39(4): 1164-1172. <https://doi.org/10.18280/ijht.390414>
- [5] Sokolnikova, P., Lombardi, P., Arendarski, B., Suslov, K., Pantaleo, A.M., Kranhold, M., Komarnicki, P. (2020). Net-zero multi-energy systems for Siberian rural communities: A methodology to size thermal and electric storage units. *Renewable Energy*, 155: 979-989. <https://doi.org/10.1016/j.renene.2020.03.011>
- [6] Huang, J., Zou, T., Li, T., Dai, B., Feng, Y. (2023). Study on discharging characteristics of solid heat storage bricks: Experiment and simulation. *Energy Reports*, 9: 1948-1962. <https://doi.org/10.1016/j.egy.2023.01.009>
- [7] Vigneshwaran, K., Sodhi, G.S., Guha, A., Muthukumar, P., Subbiah, S. (2020). Coupling strategy of multi-module high temperature solid sensible heat storage system for large scale application. *Applied Energy*, 278: 115665. <https://doi.org/10.1016/j.apenergy.2020.115665>
- [8] Cisek, P., Taler, D. (2016). Numerical and experimental study of a solid matrix Electric Thermal Storage unit dedicated to environmentally friendly residential heating system. *Energy and Buildings*, 130: 747-760. <https://doi.org/10.1016/j.enbuild.2016.08.069>
- [9] Cisek, P., Taler, D. (2019). Numerical analysis and performance assessment of the thermal energy storage unit aimed to be utilized in smart electric thermal storage (SETS). *Energy*, 173: 755-771. <https://doi.org/10.1016/j.energy.2019.02.096>
- [10] Khimenko, A.V., Tikhomirov, D.A., Kuzmichev, A.V., Trunov, S.S., Shepvalova, O.V. (2021). Thermal characteristics and operation efficiency of solid-state electro thermal storage. *Energy Reports*, 7: 219-231. <https://doi.org/10.1016/j.egy.2021.07.129>
- [11] Eggers, J.R., von der Heyde, M., Thaele, S.H., Niemeyer, H., Borowitz, T. (2022). Design and performance of a long duration electric thermal energy storage demonstration plant at megawatt-scale. *Journal of Energy Storage*, 55: 105780. <https://doi.org/10.1016/j.est.2022.105780>
- [12] Andharia, J.K., Solanki, J.B., Maiti, S. (2023). Performance evaluation of a mixed-mode solar thermal dryer with black pebble-based sensible heat storage for drying marine products. *Journal of Energy Storage*, 57: 106186. <https://doi.org/10.1016/j.est.2022.106186>
- [13] Salem, M.R., Owyed, M.N., Ali, R.K. (2023). Experimental investigation of the performance attributes of a thermal energy storage unit using different system configurations. *Applied Thermal Engineering*, 230: 120678. <https://doi.org/10.1016/j.applthermaleng.2023.120678>
- [14] Zotică, C., Pérez-Piñero, D., Skogestad, S. (2021). Supervisory control design for balancing supply and demand in a district heating system with thermal energy storage. *Computers & Chemical Engineering*, 149: 107306. <https://doi.org/10.1016/j.compchemeng.2021.107306>
- [15] Arslan, O. (2021). Performance analysis of a novel heat recovery system with hydrogen production designed for the improvement of boiler effectiveness. *International Journal of Hydrogen Energy*, 46(10): 7558-7572. <https://doi.org/10.1016/j.ijhydene.2020.11.253>
- [16] Jadwiszczak, P., Niemierka, E. (2023). Thermal effectiveness and NTU of horizontal plate drain water heat recovery unit-experimental study. *International Communications in Heat and Mass Transfer*, 147: 106938. <https://doi.org/10.1016/j.icheatmasstransfer.2023.106938>
- [17] Alqaed, S., Fouda, A., Elattar, H.F., Mustafa, J., Almeahmadi, F.A., Refaey, H.A., Alharthi, M.A. (2022). Performance evaluation of a solar heat-driven poly-generation system for residential buildings using various arrangements of heat recovery units. *Energies*, 15(22): 8750. <https://doi.org/10.3390/en15228750>
- [18] Choi, D., Gallimard, L., Sassi, T. (2015). A posteriori estimates for a natural Neumann–Neumann domain decomposition algorithm on a unilateral contact problem. *Journal of Scientific Computing*, 64: 818-836. <https://doi.org/10.1007/s10915-014-9944-8>
- [19] Ahmad, I., Zahid, H., Raja, M.A.Z., Ilyas, H., Mohayyuddin, Z. (2025). Use of Levenberg-Marquardt networks for optimization of thermal dispersion in moving triangular porous fin. *International Journal of Thermal Sciences*, 210: 109613. <https://doi.org/10.1016/j.ijthermalsci.2024.109613>
- [20] Christof, C. (2017). L_∞ -error estimates for the obstacle problem revisited. *Calcolo*, 54(4): 1243-1264. <https://doi.org/10.1007/s10092-017-0228-1>